Pereskia aculeata vibrational model by Raman characterization and DFT method

Quesle da Silva Martins
Departamento de Física, Universidade Federal de Rondônia, Ji-Paraná, R. Rio Amazonas, 351 - Jardim dos Migrantes, Ji-Paraná - RO, 76900-726.
ORCID: https://orcid.org/0000-0002-1315-2164
Email: quesle@fisica.ufmt.br

Natali Felix Arinos
Instituto de Física, Universidade Federal de Mato Grosso, Cuiabá, Av. Fernando Correa da Costa, 2.367 – Boa Esperança, 78060-900, Mato Grosso.
ORCID: https://orcid.org/0000-0003-4732-7759
Email: talifelix@fisica.ufmt.br

Cristian Aguirre Tellez
Instituto de Física, Universidade Federal de Mato Grosso, Cuiabá, Av. Fernando Correa da Costa, 2.367 – Boa Esperança, 78060-900, Mato Grosso.
ORCID: https://orcid.org/0000-0001-8064-6351
Email: cristian@fisica.ufmt.br

Jorge Luiz Brito de Faria
Instituto de Física, Universidade Federal de Mato Grosso, Cuiabá, Av. Fernando Correa da Costa, 2.367 – Boa Esperança, 78060-900, Mato Grosso.
ORCID: https://orcid.org/0000-0002-7066-6823
Email: hulk@fisica.ufmt.br

Abstract

Raman scattering was used to obtain vibrational modes in a Pereskia aculeata sample. The obtained spectrum was compared with quercetin's theoretical spectra, kaempferol, isorhamnetin, rutinose, caffeic, and tartaric acid, generated from the density functional theory (DFT) method, which used structures of the known composition present in the sample. Among the main compounds, phenolic acids and flavonoids are mentioned. Vibrational signatures, designated as CO and CH group modes, are abundant and bands in the region between 800 and 1800 cm^{-1}. This showed that the theoretical and experimental results had good correspondence between the flavonoids. Statistical observations of correlation and principal component analysis (PCA) were used, which helped in the process of correlation between sample and data obtained. Theoretical spectra have been corrected by a single scale factor of 0.961, and vibrational contributions by the molecular group were via VEDA software.

Keywords: Raman spectrum; DFT method; Ora-Pro-Nóbis; phenolic; flavonoids;

1. Introduction

The United Nations (UN) presented data on population projections, and contrary to what was previously projected, the world population is unlikely to stop growing in this century. This makes a significant increase in agricultural demand for the entire world population, inevitable to 2100 (Alstom et al., 2009; Godfray et al., 2010; Gerland et al., 2014; DESA, 2015; Rakimzhan et al., 2019). In this perspective, alternative solutions are proposed every day to minimize the impact of increasing food consumption demand. Among these alternatives, we can mention that functional foods stand out in guaranteeing nutrition because they are rich in phenolic and flavonoid compounds necessary in the human diet (Ozkan et al. 2007; Siger et al. 2008). *Pereskia aculeata*, known as Ora-Pro-Nóbis (OPN), has been indicate in recent years (Calixto et al. 2012; Pinto et al. 2015; Machado et al., 2015; Silva, 2017; Vieira et al, 2019), precisely because it contains such characteristics in food terms shown in the recent study on the existence of phenolic acids and flavonoids. Studies have shown that quercetin, isorhamnetin and kaempferol are described as the main aglycones in OPN fruits and peels. Also, references point to caffeic acid as the main phenolic constituent of the plant extract and the quercetin-3-*O*-rutinoside and isorhamnetin-3-*O*-rutinoside flavonoids (Gonçalves et al., 2015; Ferreres et al., 2017; Garcia et al. 2019; Tania, 2020). Given the potential of applications and recent studies in the identification of plant compounds, this work becomes a pioneer when carrying out an investigation by dispersive Raman spectroscopy (RS) with a plant sample, crossing information from experimental data with theoretical data obtained from density functional theory (DFT) calculations. The RS has been chosen because it is considered a specific technique capable of assisting in the plants and organic characterization process (Schulz, 2007; Gierlinger, 2007; Rakimzhan et al., 2019) and quickly obtaining information without expensive handling procedures. The computational method (DFT method) chosen is one of the most used methods to treat molecular structures' conformational and vibrational nature (Lu et al. 2013; Ramya et al., 2013; Komjati et al., 2016; Teixeira et al., 2020; Erdogdu et al., 2020). The caffeic and tartaric acid, quercetin, isorhamnetin, kaempferol and rutinose molecules were optimized in a Gaussian 03 package (Figure 1). The B3LYP Functional and 6-31G (d,p) base set has been chosen for this step. Because of an overestimated spectrum set, the calculated frequencies were adjusted by scale factor (Nist, 2020) of 0.961. Maximum energy parameters of contributions by molecular groups and the classification of vibrations collected via VEDA software are also given.

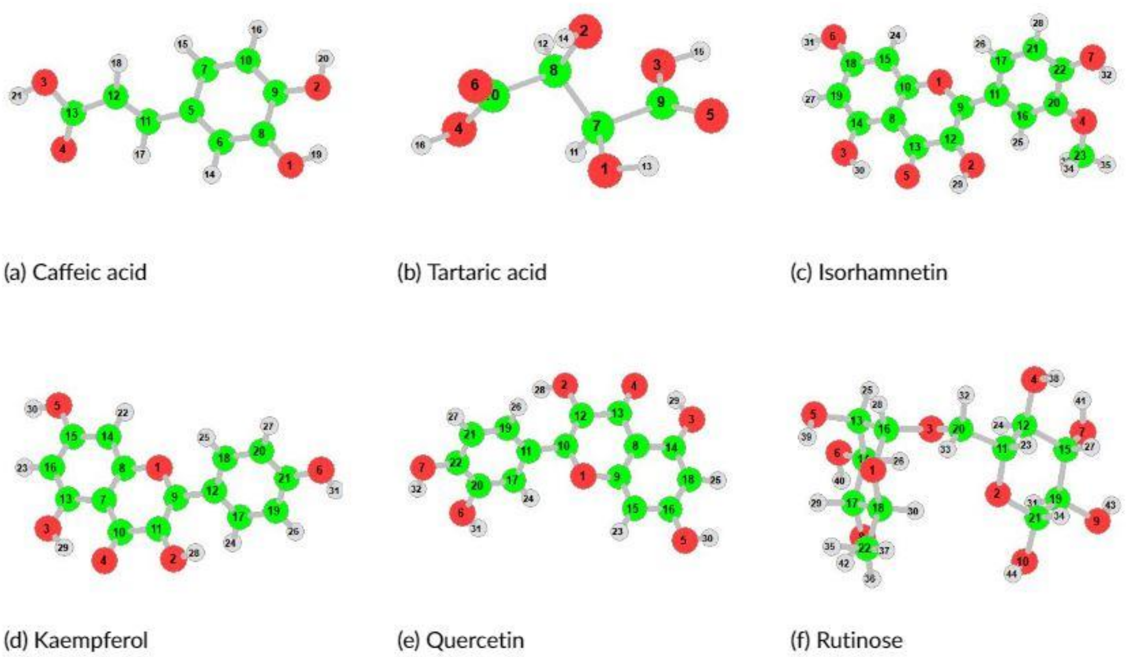

Figure 1. Molecules optimized in Gaussian by B3LYP functional and 6-31G(d,p) base set. Phenolic acids: a) Caffeic; and b) Tartaric. The c) Isorhamnetin; d) Kaempferol and e) Quercetin flavonoids. The acids a) e b) are an isolated form of Caftaric acid. Em c, d, and e, molecules isolated from Isorhamnetin-3-*O*-

rutinoside and Quercetin-3-*O*-rutinoside respectively. Em f) Rutinose, a disaccharide. In red, green, and gray, are oxygen, carbon and hydrogen respectively.

2. Material and Method

2.1 Material

The *Pereskia aculeata*, popularly known as Ora-Pro-Nóbis (OPN), is a type of Brazilian cactus. Its leaves are a great source of protein, making it superior among other vegetables, in addition to presenting basic levels of minerals, dietary fiber, vitamins, and folic acid (Souza et al., 2016; Garcia et al., 2019). This study, where a commercial brand was randomly chosen, in which a kind of organic flour made from dried OPN leaves was purchased. The sample was kept in a dry and moisture-free place and was not subjected to any RS measurement preparation.

2.2 Raman scattering

In the Raman scattering (Raman, 1929; Kalasinsky et al., 2007; Hui et al., 2019) of this study, a conventional Horiba Labram 800HR spectrometer, spectral at 80 to 4000 cm^{-1} range, single 633 nm laser was used. The Raman spectra were obtained at separate intervals of 80-1800 cm^{-1} and between 1800 and 3600 cm^{-1}, with a resolution of 2 cm^{-1}, the microscope is confocally coupled to an 800 mm focal length spectrograph, equipped with two selectable grids. The spectra were collected at room temperature in pure samples.

2.3 Computational method

The computational calculations were performed based on the functional density theory (DFT) method, whose molecular geometries were optimized with functional B3LYP and base set 6-31G(d,p) (Ditchfield, 1971; Henre, 1972; Petersson, 1991; Rassolov et al., 1998; Rassolov et al., 2001), in Gaussian Package 03 (Gaussian, 2003). The hybrid function of three parameters (B3) and Lee-Yang-Parr functional correlation (LYP) (a functional correlation that has local and non-local terms). The function has a good approach in the calculation of molecular structures and vibrational frequencies (Lee, 1988; Becke, 1993; Wu et al., 2012; Huang et al., 2016). The use of two or more scale factors is acceptable, but it necessarily depends on your data set's size and how the expected modes are different from the expected (Bauschlicher, 1997; Bauschlicher, 2010; Mattioda and Bauschlicher, 2017). The symmetries, vibrational assignments and calculations of potential energy distribution (PED) were performed with a lofty degree of accuracy. The VEDA software optimizes the set of internal coordinates for the development of experimental/theoretical IR/Raman systems. The PED calculations were performed with the support of the VEDA 4 program (Jamróz, 2004 and Jamróz, 2013).

2.4 Processing date

Experimental and theoretical results were pre-treated with multivariate analysis, through Pearson correlation and principal component analysis (PCA), which was applied in a set of pre-defined spectra in the digital printing region of the data. Correlation and PCA data were acquired using RStudio 0.4.7 software. Statistical analysis was initially used to survey differences between samples and search for a match between raw data (Bueno et al., 2017; Nazife et al., 2019).

3. *Results and Discussion*

Figures and Tables: Figures 2(a) and (b) show the Raman spectrum of the sample throughout the results. Figure 3 shows the DFT calculation results for the molecules in Figure 1. The Table 1 gives an overview of the Raman bands of the samples (experimental/theoretical) investigated. In Tables S2 to S7 (Supplementary material), the DFT calculation (GAUSSIAN and VEDA results) is observed, and Figure 4(a) and (b) shows the statistics of the frequency range and comparison.

3.1 Experimental date

The RS spectrum of OPN is shown in a research window comprising the region between 80 - 1800 cm^{-1} and between 2400 - 3600 cm^{-1} (Figure 2). What is seen initially is that this region between 80 - 1800 cm^{-1} (Figure 2(a)) shows a great density on bands of the spectrum, already in Figure 2(b), a band with overlapping basis with peaks centered at 2910 cm^{-1} and 2933 cm^{-1}.

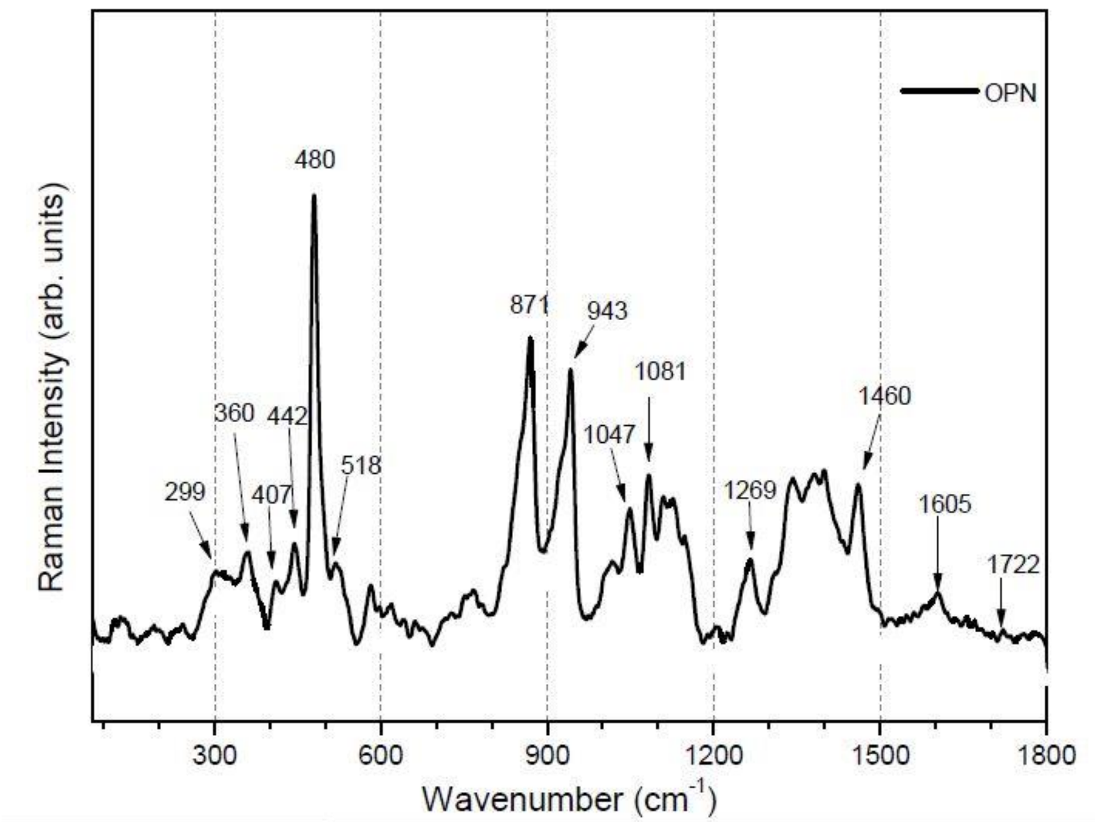

a) Measured between 80 and 1800 cm^{-1}.

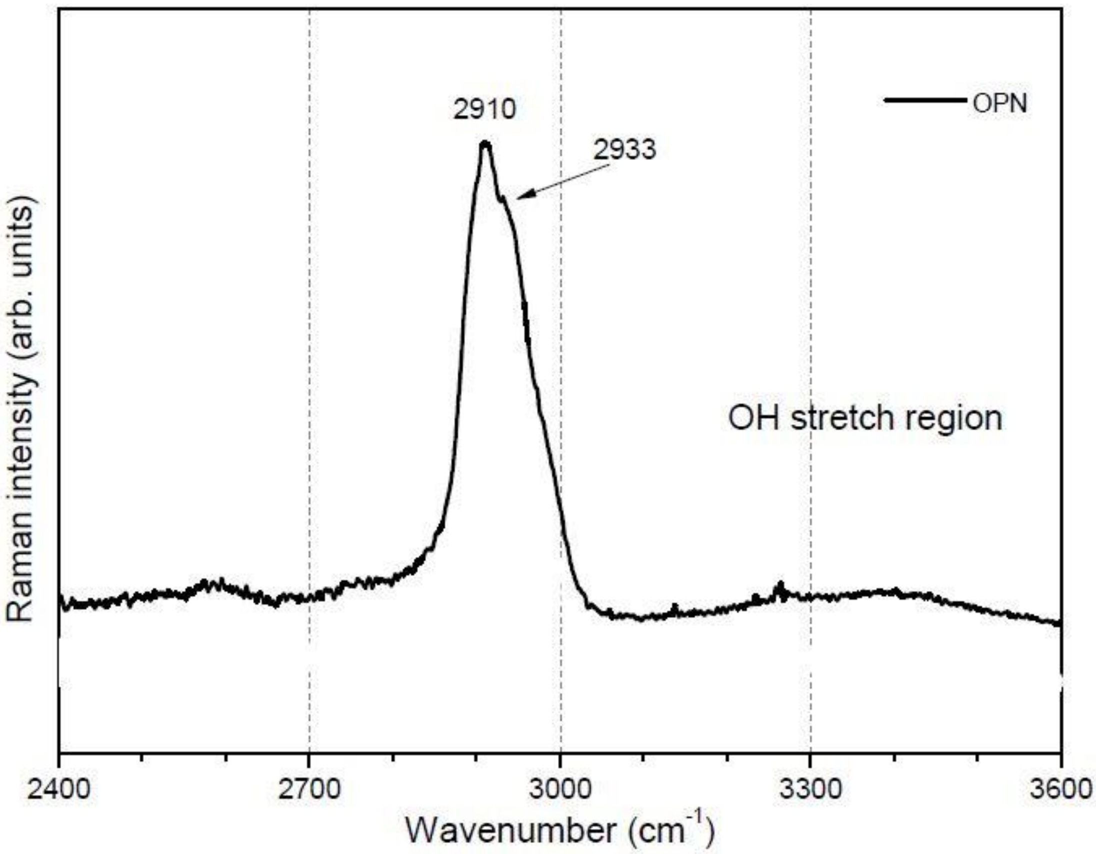

b) Measured above 2400 cm^{-1}.

Figure 2. Experimental Raman spectrum of OPN flour. The spectra were measured in different regions between: a) 80 - 1800 cm^{-1}. In b) the range from 2400 to 3600 cm^{-1} is shown.

The spectra were obtained under strong fluorescent curves of the sample, probably due to chlorophyll, typical in plants. In this case, because it is a photosynthetic pigment, chlorophyll has a strong absorption at 430 and 660 nm, precisely in the range of the laser line used in the procedure (Saleem et al., 2020). In Figure 2(a) see the peak of 480 cm^{-1}. At first, this band may be pectins, acids present in the cell walls of plants. They may be related to one of C–O–C group elongation and deformation in the range 335-900 cm^{-1} (Sene et al., 1994), where results can be linked to phenolic compounds since this band is common in rutinose, quercetin and isorhamnetin, in 484, 480 and 588 cm^{-1} respectively. The peak at 480 cm^{-1} can also be related to plant fiber lignin or cellulose; this can be explained because the region between 390 cm^{-1} and 1100 cm^{-1} vibrational bands both from lignin and cellulose coexist (Conners and Banerjee, 1995). These polysaccharides in the plant's fiber, combined with laser orientation, maybe the cause of this intense nature. Also, in this region (330-850 cm^{-1}), the band at 854 cm^{-1} may be related to deformation modes (Thygesen and Gierlinger, 2013). Thus, the peak at 871 cm^{-1} may also have some indication for deformation modes, and may be an indicator for the presence of caffeic acid, which contains HC=CH group deformations. Therefore, peaks at 871 cm^{-1} and 943 cm^{-1} can be referenced in the region indicated for the OPN sample. The commented region could be researched in the space between 450 to 1000 cm^{-1} and cite that the evidence of aromatic cyclic could reveal the existence of an atom as nitrogen. However, it would not be a sensible search since its manners would resemble those already existing, especially those of the CH group (Mattioda and Bauschlicher, 2017).

Vibrational activities at 1081, 1276, 1380, 1399, 1460 cm^{-1} that may bring references to deformations CH, COH, CO groups, and peaks of important phenolic constituents can be evidenced around 1430 cm^{-1} and at 1600 cm^{-1}, related to the stretching of aromatic compounds, in the case of flavonoids (Sene et al., 1994). Less intense markes at 1605, 1655, 1722 cm^{-1} bands would appear in an important characterization region, as they can usually bring sense to the presence of C=C, aromatic or polycyclic substitution groups, and C=O, which are normally present in organic compounds, already reported to contain antioxidant and phenolic content. Thus, isorhamnetin (1652 cm^{-1}), kaempferol (1656 cm^{-1}), and quercetin (1659 cm^{-1}) bring a good correspondence of C=C stretching modes for OPN. The region between 1000 and 1500 cm^{-1} can indicate the folding of CH_2 and CH_3 modes. Containing a significant number of carboxylic acids in the same region, it may be responsible for the possible ways of stretching and folding in RS. The bands at 357, 518, 942, 1605, and 1745 cm^{-1} may be associated with pectins and lignins (Lupoi et al., 2015; Agarwal, 2019; Makarem et al., 2019). The Figure 2(b), a wide band, overlapping two bands with center peaks at 2910 cm^{-1} and 2933 cm^{-1}, is present in the CH_2 and CH_3 stretch region. In an assignment, the methyl group may contain symmetrical and asymmetric stretching modes, and if associated with isorhamnetin (Table S3), these bands are at 3022 cm^{-1} and 3094 cm^{-1}. In the theoretical RS, associated with OH stretches, this region presents between 2750 and 3450 cm^{-1} and between 3150 and 3500 cm^{-1}.

3.1 Calculation date

The theoretical RS (T-RS) is shown in Figure 3 and reported to the structures in Figure 1, identified by capital letters.

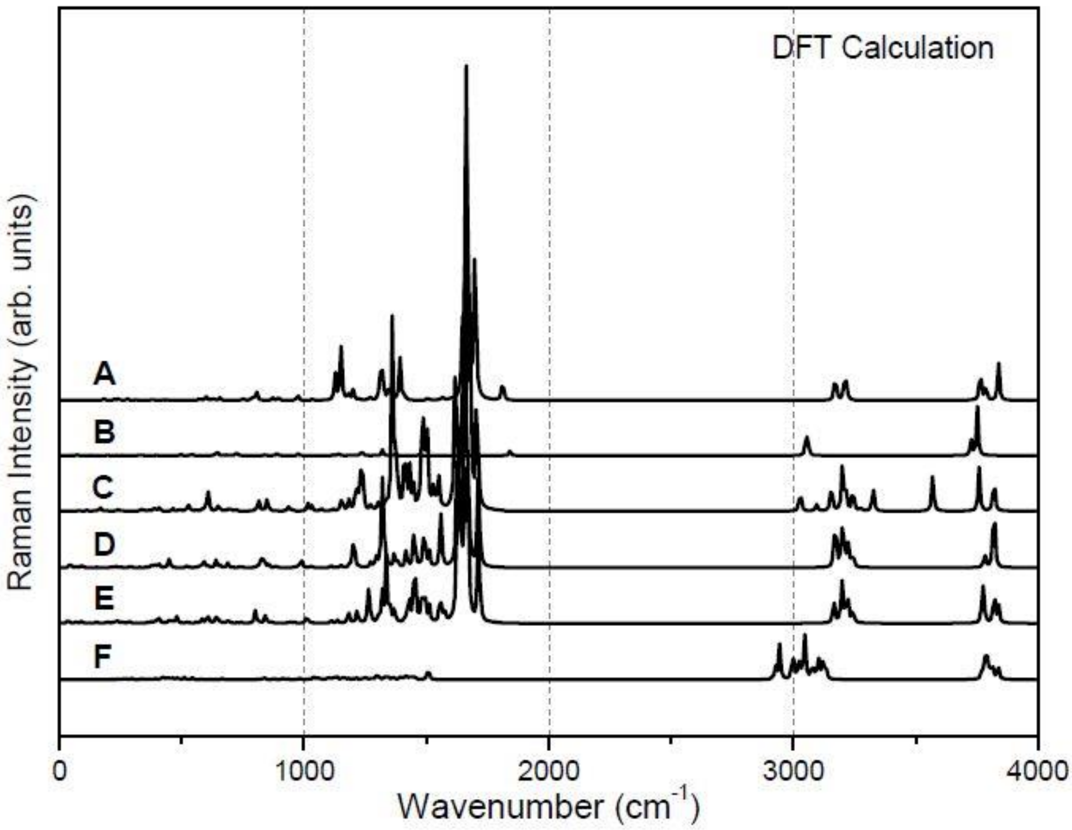

Figure 3. Raman spectra from DFT at Caffeic acid (A), Tartaric acid (B), Isorhamnetin (C), Kaempferol (D), Quercetin (E) and Rutinose (F) molecules. Functional B3LYP polarized for 631G(d,p) base set was used.

The T-RS are shown across the spectrum, between 80 cm^{-1} and 4000 cm^{-1}. The calculations show discrete bands between 3000 cm^{-1} and 4000 cm^{-1}, which can be linked to groups CH and OH. The region below 1000 cm^{-1} shows low-intensity bands, bringing important meanings since the theoretical data can bring correspondence with the experimental data. The caffeic acid structure (A), shows a planar distribution after optimization, so we can classify that the existing modes can be in the plane or outside the plane. The T-RS of A brings low intensity modes in regions below 1000 cm^{-1}, presenting out-of-the-plane deformation (torsion) modes for OH at 241 cm^{-1}. The band at 806 cm^{-1} rings an asymmetric elongation of the carbon atoms adjacent to the ring replacement. Torsion modes in the plane identified for the CH groups of the carbon and the COOH radical and at 1127 and 1150 cm^{-1}, respectively. The region between 1250 cm^{-1} and 1500 cm^{-1} bring torsion modes in the CH and OH plane all the structure. Bands of medium and high-intensity corresponding identify the bands at 1647 and 1666 cm^{-1} to the C=C connections and respective symmetrical stretching modes. At 1698 cm^{-1}, we have a symmetrical stretching mode of C=C, but this time for atoms attached to the carboxyl radical. The band at 1811 cm^{-1} reports to the C=O group with symmetrical elongation. In the region next 3800 cm^{-1}, we have 3 modes of symmetrical stretching for the OH present in the structure. The T-RS of tartaric acid (B) contains well-defined bands across the spectrum. Between 0 and 1500 cm^{-1}, a series of structure deformation modes, all related to the OH group. The band at 1840 cm^{-1} groups the symmetric stretching modes of the two existing C=O groups. Between 3000 and 3100 cm^{-1}, there are two bands, one at 3049 cm^{-1} and another at 3058 cm^{-1}, responsible for the asymmetric and symmetric stretching of CH modes. The isorhamnetin molecule (C) spectrum has bands in at 605, 814, 849 cm^{-1} with structure deformation modes. Bands between 1200 and 1500 cm^{-1} are associated with OH's angular deformations including bands at 1500 cm^{-1} methyl groups. Between 1600 and 1750 cm^{-1}, we have axial deformations of the aromatics. The bands between 300 and 3400 cm^{-1} are attached to the group CH$_{3}$ and CH, with symmetrical stretching modes in 3028 and 3275 cm^{-1}, respectively. At 3094 and 3155 cm^{-1}, asymmetric stretch modes. Bands above 3325 cm^{-1} are responsible for symmetrical stretches of OH. The kaempferol (D) shows deformation of the structure below 1000 cm^{-1}. These low-intensity but notable bands are at 449, 589, 639, 835, and 998 cm^{-1}. The 1200 cm^{-1} band may be related to the OH and CH deformation mode of the benzene group. Between 1200 and 1600 cm^{-1}, we have structural deformation related to the OH group in the molecule. At 1625 cm^{-1}, we have a symmetrical stretch of the C=C group of cyclic compounds linked to the substitution and at 1655 cm^{-1}, the most intense contribution from C=C. We have contributions located in three different bands, at 1666, 1674 and 1713 cm^{-1}, accompanied by harmonics for CC and CH. The CH symmetric and asymmetric stretching modes are found in 3225 and 3210 cm^{-1}. Two OH bands appear at 3781 and 3819 cm^{-1}. The result for quercetin (E) brings little vibrational activity below 1200 cm^{-1}. In this region, a weak band at 480 cm^{-1} (OH twist mode and ring deformation) agrees with experimental results. The band at 803 cm^{-1} (CH deformation) is one of the bands that stand out, as they correspond to a mode that covers a group HC=C=CH (linked to one of the flavonoid rings). Bands between 1200 and 1600 cm^{-1} are assigned to CH and OH deformation modes. The C=C symmetrical stretch modes are present in 1629, 1658 and 1667 cm^{-1} and correspond to the T-RS's most intense bands. The bands at 1673 and 1714 cm^{-1} indicate modes of symmetrical stretching of C=O and OH deformation. The bands around 3200 cm^{-1} bring CH stretch modes and above 3500 cm^{-1} OH symmetrical stretch modes. For rutinose (F), we have 3 distinct regions with low-intensity bands between 0 and 1500 cm^{-1}, medium and high between 2800, 3200, 3750 and 4000 cm^{-1}. The first region mentioned, with bands between 200 and 600 cm^{-1}, is linked to OH bending modes. Marked OH bands are seen at 297, 335, 353, 392, 417, 425, 443 and 461 cm^{-1}. The other bands in this region refer to the deformation of the molecule. The region between 2900 and 3200 cm^{-1} contains intense bands for CH and CH_3 presenting symmetric stretch modes in 2927, 2944, 2997, 3105, 3122 cm^{-1} for CH, and at 3047 cm^{-1} for CH_3 and asymmetric stretch mode for 3092 cm^{-1} and 3122 cm^{-1} for CH and CH$_{3}$ respectively. The bands in the 3800 cm-

[1] region are all in OH symmetrical stretch modes. Tables S2 to S7 (Supplementary Material) show the experimental and theoretical results' vibrational frequencies, accompanied by scaled frequencies (scale factor 0.961) and percentage and vibrational contribution by molecular group (PED). The vibrations in the Tables are labeled as symmetrical: (υ_s) and asymmetric (υ_{as}) and deformations in the plane: scissoring (δ_{sci}) and rocking (δ_{roc}), or out-of-plan, wagging (δ_{wag}) and twisting (δ_{twi}). In general, the result shows that the highest percentage contributions are to the OH group, generally above 90% PED. It is interesting to note that such an individual contribution does not add up to the experimental data and is considered unassigned (NA). An extensive discussion in the literature (Nyquist and Kagel, 1971; Mahesar et al., 2014; Huang et al., 2016; Larkin, 2018; Toposki, 2018; Costa et al., 2019; Hoang, 2020) bases the bands between 600 and 4000 cm^{-1}, however, below 600 cm^{-1} this is not that simple. In this sense, it uses the computational method since, in RS, we can have bands well below 500 cm^{-1}. Table 1 shows caffeine, isorhamnetin and rutinose with linked bands in the OPN sample. In the O-H stretching region, above 3100 cm^{-1}, are shown in the supplementary materials.

Table 1. Overview of the observed experimental and DFT calculations Raman bands (in cm^{-1}) and assignments of the main vibrational modes by molecular group.

OPN	Caffeic	Tartaric	Isorhamnetin	Kaempferol	Quercetin	Rutinose	Assignment
2933	-	-	3095	-	-	-	υ_s (CH)
-	-	-	-	-	-	3048	υ_s (CH)
-	-	-	-	-	-	3027	υ_s (CH)
2910	-	-	3028	-	-	3027	υ_s (CH)
1722	1812	1842	1652	1675	1674	-	υ_s (O=C)
-	1699	-	-	-	-	-	υ_s (C=C) ring
-	1667	-	-	-	1668	-	υ_s (C=C) ring
1655	1648	-	1652	1656	1659	-	υ_s (CC)
1399	1410	-	-	-	-	-	υ_s (CC)
1380	1392	1380	1378	1381	-	-	υ_s (CC)
1342	1348	1353	1336	1336	1337	1341	δ (HCC), υ_s (CC)
1267	1270	-	1274	1273	1263	1277	δ (HCC), (HOC)
1127	1128	1118	1118	-	1135	1134	δ (CCC), υOC
871	871	872	-	-	-	877	δ (HCCO), HCCC
580	580	-	588	589	582	583	δ (HOCC), (CCC)
443	-	-	-	449	443	443	δ (HOCC), υ(CC) backbone
130	138	130	-	-	-	-	δ (OCCC)

Table 1 is labeled as symmetrical (υ_s) and deformations (δ) vibrations.

3.2 Exploratory principal component analysis

The results of the E-RS (experimental) and T-RS (theoretical) combined are shown in Figure 4, which concerns Pearson's correlation, from the interaction between bands admitted in the region between 80 and 1800 cm^{-1}. Other regions that are left out of the analysis (over 2000 cm^{-1}) have a low overall signal-to-noise ratio or are composed exclusively of CH and OH bands, which are very common in organic products. The chosen region comprises the so-called digital printing region of components. The results show that the highest correlations are given between structures associated with flavonoids. These are precisely the ones that most correspond to the experimental data, with a moderate positive correlation of 0.519. All have a positive correlation between themselves (Figure 4a). The PCA was then applied to the indicated region. It was demonstrated that the total variance of the data set could be explained by seven main components, where the first two main components (Dim 1 and Dim 2), with eigenvalue greater than 1, explain approximately 64.02% of the total variance (Figure 4b). The main PCA components' highest loads showed that the main differences in sample discrimination were around 596-751 cm^{-1}, 1147-1460 cm^{-1} and 1655-1722 cm^{-1}. Bands from these regions are discriminated by twisting deformations, scissoring and stretching of OC, CC, C=C and C=O groups respectively. The PCA result was consistent when comparing E-RS and T-RS data, understanding that among the most significant components of OPN, there is association with the studied flavonoids. A prediction of this nature can be seen in Supplementary material.

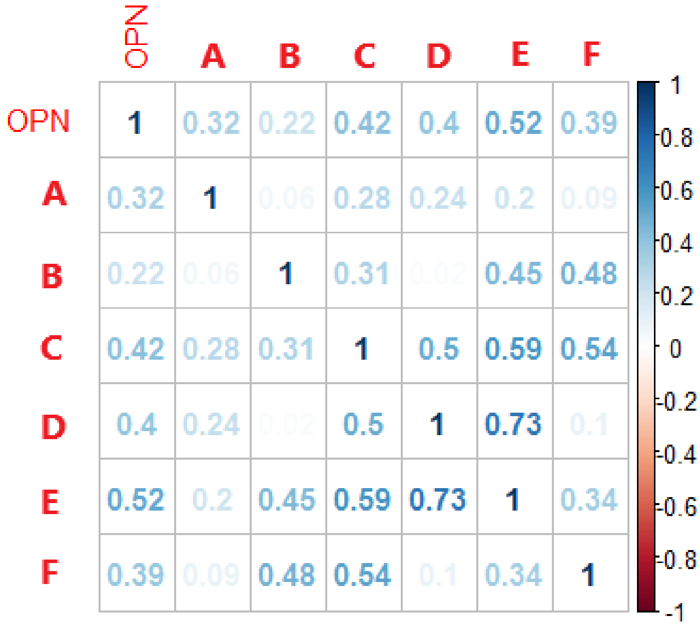

a)

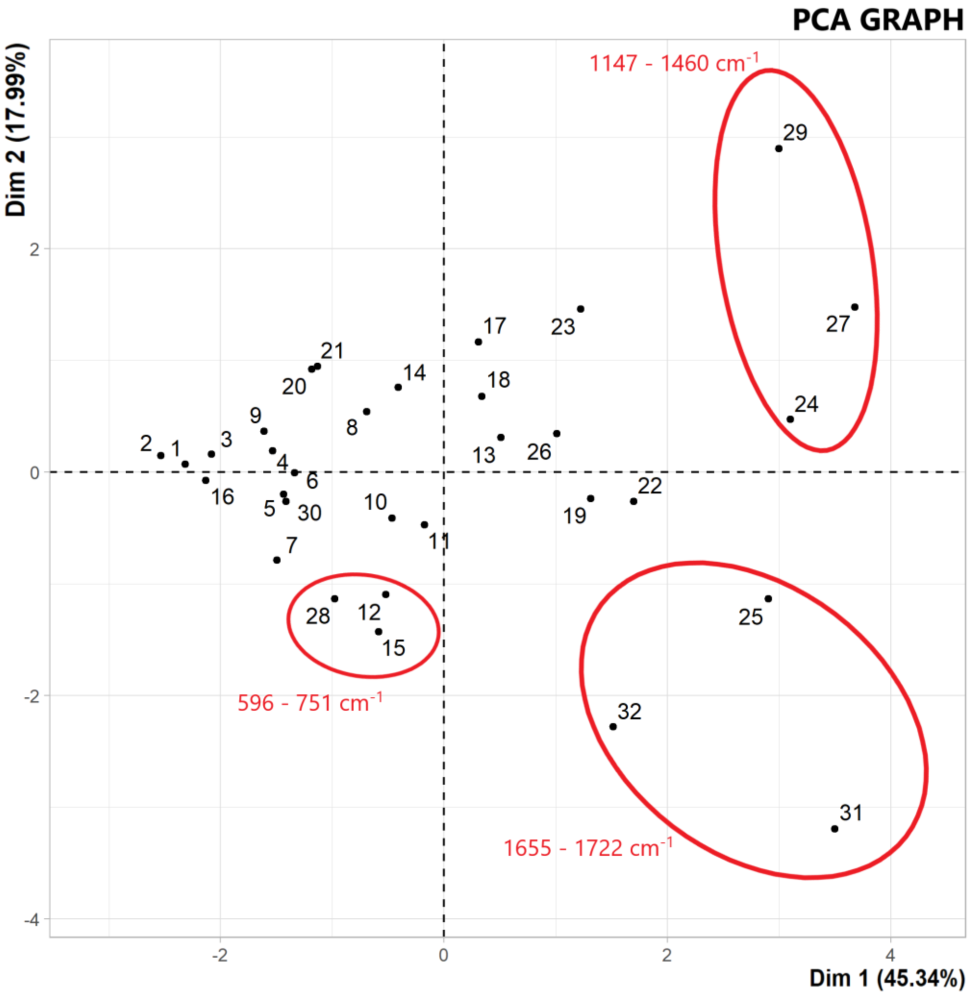

b)

Figure 4. a) Correlation graph and b) PCA data set between experimental and theoretical data from Raman spectrum. Pearson correlation obtained after 21 interactions.

4. Conclusion

Through RS, vibrational signatures of OPN were successfully acquired, and DFT data were important in discriminating these signatures. These signatures showed very significant bands at 480, 871 and 943 cm^{-1}. These bands were related to ways of deformation of plant components. Molecular groups of OC and CH bonds are quite abundant in the region below 1600 cm^{-1} due to phenolic constituents. The T-RS have low intensity bands for regions below 1200 cm^{-1} but bring important modes that relate to the experimental data. The DFT method was able to identify important bands such as C=O, between 1722 and 1750 cm^{-1} and CH_3 groups around 3000 cm^{-1}, which served as the basis for the interpretation of the experimental curve. Of the calculated constituents, phenolics showed higher affinity patterns with the OPN sample. The PCA data indicated that these correspondences are greater due to clusters in the regions of 596-751 cm^{-1}, 1147-1460 cm^{-1} and 1655-1722 cm^{-1}. The OH symmetrical stretching modes are evident in the theoretical data. Still, the experimental data is not clear because (OH) above 3200 cm^{-1} a long band is formed, which cannot be attached to the group of hydroxyl.

5. Acknowledgement

The authors would like to thank the Optics and Nanoscopy Group (GON) of the Universidade Federal de Alagoas, the Laboratório de Espalhamento de Luz of the Universidade Federal de Mato Grosso, the Grupo de Pesquisa em Estrutura da Matéria e Física Computacional of DEFIJI/UNIR and the agreement FAPERO/CAPES (Grant: 008/2018).

6. Author statement

Q.S. Martins: Conceptualization, Methodology, Project administration, Writing - Original Draft. N.F. Arinos: Data curation, Visualization, Investigation, Writing - Original draft preparation. C. Aguirre: Software, Validation, Data curation. J.L.B. Faria: Supervision, Project administration, Methodology, Writing- Reviewing and Editing.

7. Declaration of interests

The authors declare no conflict of interest relationship in this paper.

8. References

Agarwal UP, Analysis of Cellulose and LignocelluloseMaterials by Raman Spectroscopy: A Review of the Current Status, Molecules, 2019, 24, 1659. https://doi.org/10.3390/molecules24091659

Alston JM, Beddow JM, Pardey PG, Agricultural Research, Productivity, and Food Prices in the Long Run. Science, 2009, 325, 1209–1210. DOI:10.1126/science.1170451

Bauschlicher CW, Langhoff SR, The calculation of accurate harmonic frequencies of large molecules: the polycyclic aromatic hydrocarbons, a case study, Spectrochim. Acta A, 1997, 53, 1225-1240. https://doi.org/10.1016/S1386-1425(97)00022-X

Bauschlicher CW, Ricca A, On the calculation of the vibrational frequencies of polycyclic aromatic hydrocarbons, Mol. Phys., 2010, 108, 2647-2654. http://dx.doi.org/10.1080/00268976.2010.518979

Becke AD., Density-functional thermochemistry. III. The role of exact exchange, J. Chem. Phys., 1993, 98, 5648. https://doi.org/10.1063/1.464913

Bunaciu A, Aboul-Enein HY, Hoang VD, Vibrational Spectroscopy Applications in Biomedical, Pharmaceutical and Food Sciences, Copyright, Elsevier Inc., 2020, 15-36.

Calixto C, Thiemi D, Natally K, Souza P, Crestani S, Gasparotto A, Laverde U., Involvement of arginine-vasopressin in the diuretic and hypotensive effects of *Pereskia grandifolia* Haw. (Cactaceae), J. Ethnopharmacol, 2012, 144, 86-93. https://doi.org/10.1016/j.jep.2012.08.034

Conners T, Banerjee S, Surface Analysis of Paper. Ed. CRC, Mississippi, 1995.

Costa, Agostini-Costa TS., Bioactive compounds and health benefits of Pereskioideae and Cactoideae: A review, Food Chem., 2020, 327, 126961. https://doi.org/10.1016/j.foodchem.2020.126961

Costa S, Richter A, Schmidt U, Breuninger S, Hollricher O, Confocal Raman microscopy in life sciences, Morphologie, 2019, 103, 11-16. https://doi.org/10.1016/j. morpho.2018.12.003.

Desa, U., Population division working paper no. ESA/P/WP, 2015, 241.

Ditchheld R, Hehre WJ., Pople JA, Self-Consistent Molecular-Orbital Methods. IX. An Extended Gaussian-Type Basis forMolecular-Orbital Studies of OrganicMolecules, J. Chem. Phys., 1971, 54, 724.

https://doi.org/10.1063/1.1674902
Erdogdu Y, Baskose UC, Saglam S, Erdogdu M, Ogutcu H, Özçelik S., Structural, thermal, spectroscopic, electronic and biological activity properties of coumarin-153 dyes for DSSCs: A DFT benchmark study, J. Mol. Struc., 2020, 1221, 128873. https://doi.org/10.1016/j.molstruc.2020.128873

Ferreres F, Grosso C, Gil-Izquierdo A, Valentao P, Mota AT, Andrade PB., Optimization of the recovery of high-value compounds from pitaya fruit by-products using microwave-assisted extraction, Food Chem, 2017, 230, 463–474. https://doi.org/10.1016/j.foodchem.2017.03.061

Garcia AAJ, Corrêa RCG, Barros L, Pereira C, Abreu RMV, Alves MJ, Calhelha RC, Bracht A, Peralta RM, Ferreira IC, Phytochemical prole and biological activities of 'Ora-Pro-Nóbis' leaves (Pereskia aculeataMiller), an underexploited superfood from the Brazilian Atlantic Forest, Food Chem., 2019, 294, 302-308. https://doi.org/10.1016/j.foodchem.2019.05.074

Gaussian 03, Revisão C.02, MJ Frisch, GW Trucks, HB Schlegel, GE Scuseria, MA Robb, JR Cheeseman, JA Montgomery, Jr., T. Vreven, KN Kudin, JC Burant, JM Millam, SS Iyengar, J. Tomasi, V. Barone, B. Mennucci, M. Cossi, G. Scalmani, N. Rega, GA Petersson, H. Nakatsuji, M. Hada, M. Ehara, K. Toyota, R. Fukuda, J. Hasegawa, M Ishida, T. Nakajima, Y. Honda, O. Kitao, H. Nakai, M. Klene, X. Li, JE Knox, HP Hratchian, JB Cross, V. Bakken, C. Adamo, J. Jaramillo, R. Gomperts, RE Stratmann, O. Yazyev, AJ Austin, R. Cammi, C. Pomelli, JW Ochterski, PY Ayala, K. Morokuma, GA Voth, P. Salvador, JJ Dannenberg, VG Zakrzewski, S. Dapprich, AD Daniels, MC Strain, O. Farkas, DK Malick, AD Rabuck, K. Raghavachari, JB Foresman, JV Ortiz, Q. Cui, AG Baboul, S. Clifford, J.Cioslowski, BB Stefanov, G. Liu, A. Liashenko, P. Piskorz, I. Komaromi, RL Martin, DJ Fox, T. Keith, MA Al-Laham, CY Peng, A. Nanayakkara, M. Challacombe, PMW Gill, B. Johnson, W. Chen, MW Wong, C. Gonzalez e JA Pople, Gaussian, Inc., Wallingford CT, 2004.

Gerland P, Raftery AE, Ševčíková H, Li N, Gu D, World population stabilization unlikely this century, Science, 2014, 346, 234-237. DOI:10.1126/science.1257469

Gierlinger N, Schwanninger M., The potential of Raman microscopy and Raman imaging in plant research, J. Spectrosc., 2007, 21, 69. https://doi.org/10.1155/2007/498206

Godfray H, Beddington JR, Crute I, Haddad L, Lawrence D, Muir J, Pretty J, Robinson S, Thomas S, Toulmin C, Food Security: The Challenge of Feeding 9 Billion People, Science, 2010, 327, 812–818. DOI:10.1126/science.1185383

Goncalves ASM, Peixe RG, Sato A, Muzitano MF, Souza R, Machado TD, Leal I, Pilosocereus arrabidae (Byles & Rowley) of the Grumari sandbank, RJ, Brazil: Physical, chemical characterizations and antioxidant activities correlated to detection of flavonoids, Food Res. Int., 2015, 70, 110–117. https://doi.org/10.1016/j.foodres.2014.10.009

Hehre WJ, Ditchheld R, Pople JA., Self-Consistent Molecular Orbital Methods. XII. Further extensions of Gaussian type basis sets for use in molecular-orbital studies of organic-molecules, J. Chem. Phys., 1972, 56, 2257. https://doi.org/10.1063/1.1677527

Huang F, Li Y, Guo H, Xu Z, Chen J, Zhang Y, Identification of waste cooking oil and vegetable oil via Raman spectroscopy, J. Raman Spectrosc., 2016, 47, 860–864. https://doi.org/10.1002/jrs.4895

Hu R, He T, Zhang Z, Yang Y, Liu M, Safety analysis of edible oil products via Raman spectroscopy, Talanta, 2019, 191, 324-332. https://doi.org/10.1016/j.talanta.2018.08.074.

Jamróz, MH. Vibrational Energy Distribution Analysis, VEDA 4 program, Warsaw, Poland, 2004.
Jamróz MH, Vibrational Energy Distribution Analysis (VEDA): Scopes and limitations. Spectroch. Acta A, 2013, 114, 220–230. https://doi.org/10.1016/j.saa.2013.05.096

Kalasinsky KS, Hadheld T, Shea AA, Kalasinsky VF, Nelson MP, Neiss J, Drauch AJ, Vanni G, Treado P, Raman Chemical Imaging Spectroscopy Reagentless Detection and Identification of Pathogens: Signature Development and Evaluation, Anal. Chem., 2007, 79, 2658-2673. https://doi.org/10.1021/ac0700575
Karacaglar N, Bulati T, Boyaci IH, Topcu A, Raman spectroscopy coupled with chemometric methods for the discrimination of foreign fats and oils in cream and yogurt, J. Food Drug Anal., 2019, 27, 101-110. https://doi.org/10.1016/j.jfda.2018.06.008

Komjáti B, Urai Á, Hosztah S, Kökösi J, Kováts B, Nagy J, Horváth P., Systematic study on the TD-DFT calculated electronic circular dichroism spectra of chiral aromatic nitro compounds: A comparison of B3LYP and CAM-B3LYP, Spectrochim. Acta A, 2016, 155, 95-102. https://doi.org/10.1016/j.saa.2015.11.002
Larkin P, Infrared and Raman Spectroscopy: Principles and Spectral Interpretation, 2nd ed., Elsevier, 2018.

Lee C, Yang W, Parr RG, Development of the Colle-Salvetti correlation-energy formula into a functional of the electron density, Phys. Rev. B, 1988, 37, 785. https://doi.org/10.1103/PhysRevB.37.785

Lu L, Hu H, Hou H, Wang B., An improved B3LYP method in the calculation of organic thermochemistry and reactivity, Comput. Theor. Chem., 2013, 1015, 64-71. https://doi.org/10.1016/j.comptc.2013.04.009

Lupoi J, Gjersing E, Davis EM, Evaluating Lignocellulosic Biomass, Its Derivatives, and Downstream Products with Raman Spectroscopy, Frente. Bioeng. Biotechnol., 2015, 3, 50. https://www.frontiersin.org/article/10.3389/ fbioe.2015.00050
Machado DC, Pinto ND, Silva JM, Conegundes JLM, Gualberto ACM, Gameiro J, Scio E., Pereskia aculeata: A plant food with antinociceptive activity, Pharm. Biol. 2015, 1, 1780-1785. https://doi.org/10.1016/j.jep.2015.07.032

Mahesar SA, Sherazi S, Khaskheli AR, Kandhro AA, Uddin S, Analytical approaches for the assessment of free fatty acids in oils and fats, Anal. Methods, 2014, 6, 4956-4963. https://doi.org/10.1039/C4AY00344F

Makarem M, Lee CM, Kahe K, Huang S, Chae I, Yang H, Kubicki JD, Kim SH, Probing cellulose structures with vibrational spectroscopy, Cellulose, 2019, 26, 35–79. https://doi.org/10.1007/s10570-018-

2199-z

Mattioda A, Bauschlicher CW, Infrared spectroscopy of matrix-isolated neutral polycyclic aromatic nitrogen heterocycles: The acridine series, Spectrochim. Acta A, 2017, 181, 286–308. http://dx.doi.org/10.1016/j.saa.2017.03.044

NIST, National Institute of Standards and Technology, 2020. https://cccbdb.nist.gov/vibscalejust.asp

Nogales-Bueno J, Baca-Bocanegra B, Rooney A, Hernández-Hierro JM, Byrne HJ, Heredia FJ, Study of phenolic extractability in grape seeds by means of ATR-FTIR and Raman spectroscopy. Food Chem., 2017, 232, 602-609. https://doi.org/10.1016/j.foodchem.2017.04.049

Nyquist RA, Kagel RO, Handbook of infrared and Raman spectra of inorganic compounds and organic salts: infrared spectra of inorganic compounds, Academic press inc., 1971.

Ozkan G, Sagdic O, Ekici L, Ozturk I, Ozkan M, J., Phenolic compounds of Origanum sipyleum L. extract, and Its antioxidant and antibacterial activities, J. Food Lipids, 2007, 14, 157-169. https://doi.org/10.1111/j.1745-4522.2007.00077.x

Petersson GA, Al-Laham M., A complete basis set model chemistry. II. Open-shell systems and the total energies of the rst-row atoms, J. Chem. Phys., 1991, 94, 6081-90. https://doi.org/10.1063/1.460447

Pinto N, Duque A, Pacheco N, Mendes R, Motta E, Bellozi P. Scio E, Pharm. Biol. 1, 2015 1780-1785. https://doi.org/10.3109/13880209.2015.1008144

Rakymzhan A, Yakupov T, Yelemessova Z, Bukasov R, Yakovlev VV, Utegulov ZN, Time-resolved assessment of drying plants by Brillouin and Raman spectroscopies, J. Raman Spectrosc. 2019, 50, 1881-1889. https://doi.org/10.1002/jrs.5742

Raman CV, Krishnan KS., The production of new radiations by light scattering. Part I Proc. R. Soc. Lond. A. Math., 1929, 122, 23-35. http://dspace.rri.res.in/handle/2289/2143

Ramya T, Gunasekaran S, Ramkumaar GR., Density functional theory, restricted Hartree – Fock simulations and FTIR, FT-Raman and UV–Vis spectroscopic studies on lamotrigine, Spectrochim. Acta A, 2013, 114, 277-283. https://doi.org/10.1016/j.saa.2013.05.057

Rassolov VA, Pople JA, Ratner MA, Windus TL., 6-31G* basis set for atoms K through Zn, J. Chem. Phys.,1998, 109, 1223-29. https://doi.org/10.1063/1.476673

Rassolov VA, Ratner MA, Pople JA, Redfern PC, Curtiss L, 6-31G* Basis Set for Third-Row Atoms. J. Comp. Chem., 2001, 22, 976-984. https://doi.org/10.1002/ jcc.1058

Saleem M, Atta BM, Ali Z, Bilal M, Laser-induced fluorescence spectroscopy for early disease detection in grape fruit plants, Photochem. Photobiol. Sci., 2020, 19, 713–721. https://doi.org/10.1039/C9PP00368A

Saraiva AGQ, Saraiva GD, Albuquerque RL, Nogueira CES, Teixeira AMR, Lima LB, Cruz BG, Sousa F., Chemical analysis and vibrational spectroscopy study of essential oils from Lippia sidoides and of its

major constituent, Vib. Spectrosc., 2020, 110, 103111. https://doi.org/10.1016/j.vibspec.2020.103111
Schulz H, Baranska M., Identification and quantification of valuable plant substances by IR and Raman spectroscopy, Vib. Spectrosc., 2007, 43, 13-25. https://doi.org/10.1016/j.vibspec.2006.06.001

Sene C, McCann MC, Wilson RH, Grinter R, Fourier-transform Raman and Fourier-transform infrared spectroscopy – an investigation of 5 higher plant cell walls and their components, Plant Physiology, 1994, 106, 1623–1631. https://doi.org/10.1104/pp.106.4.1623

Siger A, Nogala-Kalucka M, Lampart-Szczapa E., The content and antioxidant activity of phenolic compounds in cold pressed plant oils, J. Food Lipids, 2008, 15, 137-149. https://doi.org/10.1111/j.1745-4522.2007.00107.x
Silva DO, Seifert M, Nora FR, Bobrowski VL, Freitag RA, Kucera HR, Gaikwad NW, Acute Toxicity and Cytotoxicity of Pereskia aculeata, a Highly Nutritious Cactaceae Plant, J. Med. Food, 2017, 20, 403-409. https://doi.org/10.1089/jmf.2016.0133

Souza LF, Caputo L, Barros IBI, Fratianni F, Nazzaro F, De Feo V., Pereskia aculeata Muller (Cactaceae) Leaves: Chemical Composition and Biological Activities, Int. J.Mol. Sci., 2016, 17, 1478. https://doi.org/10.3390/ ijms17091478

Thygesen GL, Gierlinger N, The molecular structure within dislocations in Cannabis sativa bres studied by polarised Raman microspectroscopy, J. Struc. Biol., 2013, 182, 219–225. https://doi.org/10.1016/j.jsb.2013.03.010

Toporski J, Dieing T, Hollricher O, Confocal Raman microscopy (2nd ed.), Springer Series in Surface Sciences (66), Springer International Publishing AG, 2018.

Vieira CR, Silva BP, Carmo MAV., Effect of Pereskia aculeata Mill. in vitro and in overweight humans: A randomized controlled trial, J. Food Biochem., 2019, 43, e12903. https://doi.org/10.1111/jfbc.12903
Wu X, Gao S, Wang JS, Wang H, Huanga YW, Zhaod Y, The surface-enhanced Raman spectra of aflatoxins: spectral analysis, density functional theory calculation, detection and differentiation. Analyst, 2012, 137, 4226-34. https://doi.org/10.1039/ c2an35378d

Supplementary material

In Tables S2 to S7, a set of experimental, theoretical (theoretical GAUSSIAN and VEDA) and scaled (0.961 scale factor) Raman frequencies is observed from the molecules in the Figure 1 mentioned. Vibrational mode assignments by molecular group and % PED contribution and Parameter maximum energy (EPM) also shown. The vibrations in the Tables are labeled as symmetrical: (υ_s) and asymmetric (υ_{as}) and deformations (torsion) in the plane: scissoring (δ_{sci}) and rocking (δ_{roc}), or out-of-plan, wagging (δ_{wag}) and twisting (δ_{twi}).

TABLE S2 Set of experimental, theoretical and scaloned (scale factor 0.961) Raman frequencies of caffeic acid. Assignments of vibrational modes by molecular group and contribution % PED.

ω**E-SR**	ω**T-SR**	**SF 0.961**	**Assignment PED %**
NA	3839	3689	υ_s OH (2 20) 100
NA	3764	3617	υ_s OH (3 21) 100
NA	3206	3080	υ_s CH (6 14) 95
NA	3170	2986	υ_s CH (11 17) 99
1722	1812	1741	υ_s O=C (4 13) 80
NA	1699	1632	υ_s $C{=}C_{ring}$ (11 12) 52
NA	1667	1602	υ_s $C{=}C_{ring}$ (6 8) 31
1655	1648	1584	υ_s CC (10 9) 19
1399	1410	1355	υ_s CH CC (5 7) 11
1380	1392	1338	υ_s CC (5 7) 20
1342	1448	1295	δ_{sci} HCC (17 11 12) 25
1267	1270	1220	δ_{sci} HOC (18 12 13) 40
1127	1128	1084	δ_{sci} CCC (7 10 9) 16
871	871	837	δ_{twi} HCCO (18 12 13 3) 37
580	580	557	δ_{twi} HOCC (21 3 13 12) 41
130	138	132	δ_{twi} OCCC (3 13 12 11) 52

Caffeic acid. Average max. Potential Energy <EPm> = 43.915

TABLE S3 Set of experimental, theoretical and scaloned (scale factor 0.961) Raman frequencies of tartaric acid. Assignments of vibrational modes by molecular group and contribution % PED.

ω**E-SR**	ω**T-SR**	**SF 0.961**	**Assignment PED %**
NA	3727	3582	υ_s OH (1 13) 37 + (2 14) 62
NA	3727	3582	υ_{as} OH (2 14) 62 + (1 13) 37
NA	3752	3606	υ_s OH (3 15) 61 + (4 16) 39
NA	3752	3606	υ_{as} OH (4 16) 39 + (3 15) 61
NA	3058	2939	c,CH (8 12) 58 + (7 11) 37
NA	3050	2931	υ_{as} CH (8 12) 34 + (7 11) 55
1722	1842	1770	υ_s O=C (5 9) 36 + (6 10) 49
NA	1839	1767	υ_{as} O=C (5 9) 49 + (6 10) 36
1460	1452	1395	δ_{sci} HOC (13 1 7) 26
1380	1380	1326	δ_{sci} HCO (11 7 1) 15
1342	1353	1300	δ_{sci} HOC (14 2 8) 14
1311	1320	1668	δ_{sci} HCO (12 8 2) 17
1147	1141	1090	υ_s OC (1 7) 24
1127	1118	1074	υ_s OC (8 2) 32
871	872	837	υ_s CC (10 8) 20
190	195	187	δ_{tor} OCC (3 9 7) 11
130	130	125	δ_{tor} CCC (10 8 7) 20

Tartaric acid. Average max. Potential Energy <EPm> = 30.203

TABLE S4 Set of experimental, theoretical and scaloned (scale factor 0.961) Raman frequencies of isorhamnetin. Assignments of vibrational modes by molecular group and contribution % PED.

ω**E-SR**	ω**T-SR**	**SF 0.961**	**Assignment PED %**
NA	3820	3671	υ_s OH (6 31) 100
NA	3759	3612	υ_s OH (7 32) 100
NA	3570	3430	υ_s OH (2 29) 99
NA	3326	3196	υ_s OH (3 30) 99
NA	3245	3118	υ_s CH (15 24) 100
NA	3275	3147	υ_s CH (16 25) 100
NA	3242	3115	υ_s CH (17 26) 94
NA	3200	3075	υ_s CH (19 27) 100
NA	3213	3088	υ_s CH (21 28) 94
2933	3095	2974	υ_{as} CH3 (23 33) 50
2910	3028	2910	υ_s CH3 (23 34) 44
NA	1678	1612	υ_s C=C (12 9) 36
1722	1652	1587	υ_s O=C (5 13) 18
1655	1652	1587	υ_s C=C*ri ng* (18 15) 22
NA	1519	1469	δ_{sci} CH3 (34 23 33) 56
NA	1501	1442	δ_{sci} CH3 (35 23 33) 19
1460	1470	1413	υ_s CC (16 20) 10
1380	1378	1324	υ_s CC (15 10) 15
1342	1336	1284	υ_s CC (11 17) 15
1267	1274	1224	δ_{sci} HOC (31 6 18) 21
1147	1151	1106	δ_{sci} HCC (24 15 18) 12
1127	1118	1074	υ_s OC (1 10) 15
1081	1070	1028	υ_s OC (4 23) 51
1016	1016	976	υ_s CC (19 18) 17
943	950	913	δ_{twi} HCCC (26 17 21 22) 46
618	616	592	δ_{twi} OCCC (3 19 8 14) 24
580	588	565	δ_{sci} OCC (6 18 19) 14
243	241	232	δ_{twi} HOCC (19 18 15 10) 22
190	188	181	δ_{twi} CCCC (16 20 22 21) 32

Isorhamnetin. Average max. Potential Energy <EPm> = 37.152

TABLE S5 Set of experimental, theoretical and scaloned (scale factor 0.961) Raman frequencies of kaempferol. Assignments of vibrational modes by molecular group and contribution % PED.

ωE-SR	**ωT-SR**	**SF 0.961**	**Assignment PED %**
NA	3782	3634	υ_s OH (2 28) 100
NA	3821	3672	υ_s OH (5 30) 99
NA	3820	3671	υ_s OH (6 31) 99
NA	3167	3043	υ_s OH (3 29) 98
NA	3244	3117	υ_s CH (14 22) 100
NA	3198	3073	υ_s CH (16 23) 99
NA	3204	3079	υ_s CH (17 24) 93
NA	3225	3099	υ_s CH (18 25) 63
NA	3174	3050	υ_s CH (19 26) 93
1722	1675	1610	υ_s O=C (4 10) 23
1655	1656	1591	υ_s C=C (11 9) 34
1460	1451	1394	δ_{twi} HOC (29 3 13) 17
1380	1381	1327	δ_{twi} HOC (31 6 21) 21
1342	1336	1284	υ_s CC (12 17) 23
1267	1273	1223	δ_{twi} HOC (30 5 15) 28
1147	1152	1107	δ_{twi} HCC (22 14 15) 12
1016	1026	986	υ_s CC (15 14) 13
661	657	631	δ_{sci} CCC (17 19 21) 22
618	625	601	δ_{twi} HCCC (23 16 15 14) 11
580	589	566	δ_{sci} CCC (13 16 15) 19
443	449	431	δ_{twi} HOCC (28 2 11 9) 43
120	118	133	δ_{twi} CCCC (16 15 14 8) 23

Kaempferol. Average max. Potential Energy <EPm> = 34.350

TABLE S6 Set of experimental, theoretical and scaloned (scale factor 0.961) Raman frequencies of quercetin. Assignments of vibrational modes by molecular group and contribution % PED.

ω**E-SR**	ω**T-SR**	**SF 0.961**	**Assignment PED %**
NA	3772	3625	υ_s OH (2 28) 100
NA	3821	3672	υ_s OH (5 30) 100
NA	3839	3689	υ_s OH (6 31) 100
NA	3777	3630	υ_s OH (7 32) 100
NA	3166	3042	υ_s OH (3 29) 99
NA	3243	3116	υ_s CH (15 23) 100
NA	3197	3072	υ_s CH (17 24) 99
1722	1674	1647	υ_s O=C (4 13) 17
1655	1659	1594	υ_s C=C (12 10) 28
1460	1452	1395	υ_s CC (18 16) 12
1342	1337	1285	δ_{sci} HCC (26 19 21) 13
1267	1263	1214	δ_{sci} HCC (23 15 16) 22
1147	1143	1098	υ_s CC (21 19) 12
1127	1135	1091	$\delta_{r\ oc}$ HOC (31 6 20) 14
1109	1112	1069	δ_{sci} CCC (13 8 14) 16
1016	1011	971	υ_s CC (18 16) 13
728	726	698	δ_{sci} CCO (12 10 1) 12
661	659	633	$\delta_{w\ ag}$ OCCC (6 17 22 20) 17
618	619	595	$\delta_{w\ ag}$ OCCC (3 8 18 14) 27
580	582	559	δ_{sci} CCC (14 18 16) 14
480	480	461	δ_{sci} OCC (7 22 21) 13
443	443	426	δ_{twi} HOCC (28 2 12 10) 31
243	242	232	δ_{twi} HOCC (31 6 20 17) 80
190	196	188	δ_{twi} CCCC (21 19 11 17) 28

Quercetin. Average max. Potential Energy <EPm> = 32.220

TABLE S7 Set of experimental, theoretical and scaloned (scale factor 0.961) Raman frequencies of rutinose. Assignments of vibrational modes by molecular group and contribution % PED.

*ω*E-SR	*ω*T-SR	SF 0.961	Assignment PED %
NA	3798	3650	υ_s OH (4 38) 98
NA	3784	3636	υ_s OH (5 39) 99
NA	3789	3641	υ_s OH (6 40) 100
NA	3786	3638	υ_s OH (7 41) 98
NA	3796	3645	υ_s OH (9 43) 100
NA	3133	3111	υ_{as} CH3 (22 37) 73
NA	3122	3000	υ_s CH (12 24) 96
NA	3105	2984	υ_s CH (13 25) 97
NA	3076	2956	υ_s CH (18 30) 93
NA	3093	2972	υ_s CH (20 33) 81
2933	3047	2928	υ_s CH3 (22 35) 47
2910	3026	2909	υ_s CH2 (20 32) 77
NA	2927	2813	υ_s CH (11 23) 73
NA	2944	2829	υ_s CH (21 34) 85
1460	1453	1301	δ_{sci} HCO (40 6 14) 10
1342	1341	1289	δ_{twi} HCO (34 21 10) 32
1267	1277	1227	δ_{sci} HOC (41 7 15) 14
1147	1154	1109	υ_s OC (2 11) 22
1127	1134	1090	υ_s OC (9 19) 29
1081	1075	1033	υ_s CC (17 14) 16
1016	1022	982	υ_s CC (21 19) 20
871	877	843	υ_s CC (14 13) 19
661	666	640	δ_{twi} OCCC (5 14 16 13) 13
871	877	843	υ_s CC (14 13) 19
580	583	560	δ_{twi} COCC (11 2 21 19) 13
480	484	465	δ OCC (6 14 17) 12
443	443	426	δ_{tor} HOCC (40 6 14 13) 41
361	361	345	δ CCO (22 18 1) 14
248	243	233	δ_{sci} OCC (6 14 17) 12
120	124	119	δ_{wag} CCCC (17 14 13 16) 27

Rutinose. Average max. Potential Energy <EPm> = 32.966